ACS APPLIED MATERIALS & INTERFACES

Research Article

www.acsami.org

Near Room Temperature, Fast-Response, and Highly Sensitive Triethylamine Sensor Assembled with Au-Loaded ZnO/SnO_2 Core–Shell Nanorods on Flat Alumina Substrates

Dian-Xing Ju, Hong-Yan Xu, Zhi-Wen Qiu, Zi-Chao Zhang, Qi Xu, Jun Zhang, Jie-Qiang Wang, and Bing-Qiang Cao*

Laboratory of Inorganic Functional Materials, School of Materials Science and Engineering, University of Jinan, Jinan 250022, Shandong, China

Supporting Information

ABSTRACT: Chemiresistive gas sensors with low power consumption, fast response, and reliable fabrication process for a specific target gas have been now created for many applications. They require both sensitive nanomaterials and an efficient substrate chip for heating and electrical addressing. Herein, a near room working temperature and fast response triethylamine (TEA) gas sensor has been fabricated successfully by designing gold (Au)-loaded ZnO/SnO_2 core–shell nanorods. ZnO nanorods grew directly on Al_2O_3 flat electrodes with a cost-effective hydrothermal process. By employing pulsed laser deposition (PLD) and DC-sputtering methods, the construction of Au nanoparticle-loaded ZnO/SnO_2 core/shell nanorod heterostructure is highly controllable and reproducible. In comparison with pristine ZnO, SnO_2, and Au-loaded ZnO, SnO_2 sensors, Au-ZnO/SnO_2 nanorod sensors exhibit a remarkably high and fast response to TEA gas at working temperatures as low as 40 °C. The enhanced sensing property of the Au-ZnO/SnO_2 sensor is also discussed with the semiconductor depletion layer model introduced by Au-SnO_2 Schottky contact and ZnO/SnO_2 N–N heterojunction.

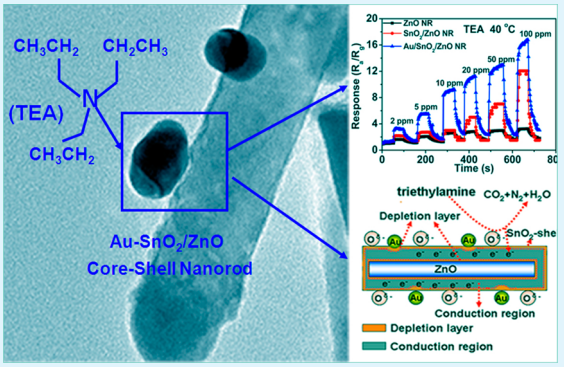

KEYWORDS: *Au-SnO_2/ZnO nanorod, Schottky contact, N–N heterojunction, TEA sensor, near room-temperature*

1. INTRODUCTION

Triethylamine (TEA) is one of the most important organic amines and has been widely used as an organic solvent, preservative, catalyst, and synthetic dye.[1,2] TEA, together with dimethylamine (DMA), trimethylamine (TMA), and ammonia (NH_3), can also be secreted in dead fish and sea creatures during their deterioration process, and the concentrations and ratios of these gases are markedly dependent on the kind of fish and freshness.[3,4] However, TEA is extremely toxic and can cause great damage to human health, such as skin burns, headaches, nausea, eye irritation, and even death. The threshold limit of TEA concentration in the air is 10 ppm on a volumetric basis (ppmV).[5] Hence, it is quite important to realize the rapid, online, trace detection of TEA. Nowadays, several methods such as gas/liquid/solid chromatography and colorimetric methods have been used to detect TEA gas in the environmental field.[2,6,7] Although the detection efficiency is high, the expensive and complex equipment required hinders its convenient application.[8] Thus, there is an urgent need to develop new TEA sensors with fast response and good selectivity for the biomedical, chemical, and food industries and also our daily life.[9]

Semiconducting metal oxide nanostructures offer a promising platform for chemiresistive gas sensors with several advantages in terms of low cost, simple fabrication, and good compatibility with microelectronic processes.[10−12] Metal oxide semiconductors such as ZnO,[13] SnO_2,[11,14] WO_3,[15] and In_2O_3[16] with nanowire, nanorod, and nanosheet morphologies have been extensively investigated for gas sensor applications. Particularly, ZnO and SnO_2,[17−19] have exhibited good sensing property to C_2H_5OH,[13,20] CO,[21] NH_3,[22,23] H_2S, and so on.[19,24] For TEA gas sensor applications, Wang et al.[25] fabricated a SnO_2 nanorod sensor to detect TEA at 350 °C. Then, our group fabricated a TEA sensor by designing NiO/ZnO PN heterojunction.[2] The best working temperature was also as high as 320 °C. Generally, ZnO or SnO_2 oxide gas sensors can work only at high temperatures of 300–400 °C to achieve or activate a reversible response to target gases. This leads to high power consumption and fast device failure due to the growth of small oxide grains and even results in ignition of flammable and explosive gases.[26] Therefore, the fabrication of gas sensors with a low working temperature is still highly desirable.[11]

Recently, it has been reported that precious metals decorated on both oxide semiconductors and heteronanostructures

Received: June 4, 2015
Accepted: August 17, 2015
Published: August 17, 2015

DOI: 10.1021/acsami.5b04904
ACS Appl. Mater. Interfaces 2015, 7, 19163−19171

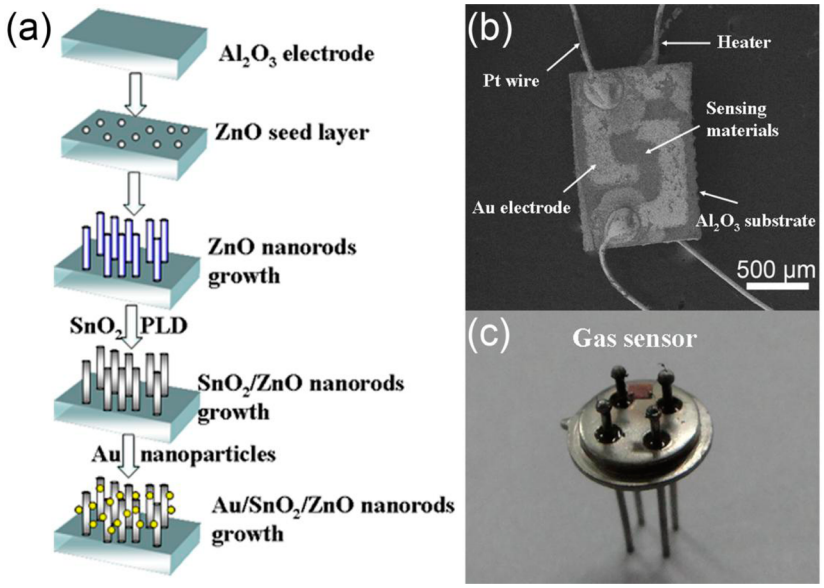

Figure 1. (a) Schematic for the growth process of Au-loaded SnO_2/ZnO core−shell nanorods. (b) SEM image of a sensor element: flat Al_2O_3 ceramic substrates (1.5 mm in length, 1.0 mm in width) with four electrodes, for example, a pair of Au electrodes attached with Pt lead wires. (c) Gas sensor of Au-SnO_2/ZnO nanorods fixed on an electronic bracket.

consisting of two or more metal oxides can improve the sensing performance. The sensing mechanism can be explained by the Schottky contact or spillover effect of precious metals and the change of resistance caused by the formation of a heterojunction. For example, Li et al.[27] synthesized Au@ZnO yolk−shell nanospheres, and their response to 100 ppm of acetone was about 2−3 times higher than that of ZnO hollow nanorods. Tang et al.[28] prepared SnO_2-ZnO composite nanofibers, which exhibited better selectivity to methanol than pure ZnO and SnO_2. Kaneti et al.[29] developed a solvothermal strategy for the synthesis of ZnO-decorated α-Fe_2O_3 nanorods, which also exhibited good sensitivity, selectivity, and stability toward *n*-butanol gas at 225 °C. Despite the high response of the above sensors, it is inconvenient to fabricate these sensors with the traditional slurry-coating fabrication process. These sensors are always assembled by two steps, including the synthesis of sensing materials and then coating them onto Al_2O_3 electrodes.[13] Obviously, such a fabrication process is time-consuming and sometimes will destroy the intrinsic nanostructure physical properties. Thus, to simplify the traditional fabrication process of gas sensors, synthesis of sensing materials directly onto the generally used flat Al_2O_3 substrates with predesigned electrodes is a promising strategy.

This work includes the design and growth of Au-SnO_2/ZnO composite nanorods for the first time to enhance the sensing performance of TEA at a reasonably low operating temperature (~40 °C). The pristine ZnO, SnO_2/ZnO, and Au-SnO_2/ZnO nanorods are grown directly on Al_2O_3 flat electrodes by combination of a hydrothermal method, pulsed laser deposition, and DC-sputtering process, which can be used directly for gas sensors without the slurry-coating process. The test results indicate that the Au-SnO_2/ZnO composite nanorod sensor exhibits an ultrafast response (~1.2 s), good stability, and a dramatic response enhancement to TEA at near room temperature (~40 °C). The sensing performances and their gas sensing mechanism are discussed in detail in the following sections.

2. EXPERIMENTAL SECTION

2.1. Direct Growth of ZnO Nanorods on Al_2O_3 Substrates. All reagents were purchased from Sinopharm Chemical Reagent (Shanghai, China). In a typical experiment, cleaned flat Al_2O_3 ceramic substrates with predesigned electrodes were immersed into a 0.01 mol/L $Zn(Ac)_2$ solution for 4 h. Then they were annealed at 350 °C for 30 min to form a ZnO seed layer. A mixed aqueous solution of 0.025 M zinc nitrate and 0.025 M hexamethylenetetramine ($C_6H_{12}N_4$) was transferred into a Teflon-lined stainless steel autoclave. Afterward, flat Al_2O_3 substrates with a seed layer were suspended into the above aqueous solution, heated to 95 °C for 3 h, and then cooled to room temperature. Finally, pure ZnO nanorods were obtained after several washings with deionized water and ethanol.

2.2. Growth of SnO_2/ZnO Core−Shell Nanorods and Loading of Au Nanoparticles. A shell layer of SnO_2 nanoparticles was deposited onto the surface of ZnO nanorods by PLD using SnO_2 target at room temperature. A KrF laser of 1 mJ/cm^2 and an oxygen partial pressure of 3×10^{-4} Pa were typically applied. By controlling the laser pulses of 500 pulses, SnO_2/ZnO core−shell nanorod heterojunctions were grown on Al_2O_3 substrates. After that, Au nanoparticles were loaded onto the core−shell nanorods by DC-sputtering with a working time of 30 s.

2.3. Material Characterizations and Sensor Properties. The morphology microstructure and composition of Au-SnO_2/ZnO nanorods were measured by a field emission scanning electron microscope (FESEM, FEI QUANTA FEG250) equipped with energy dispersive X-ray spectroscopy (EDS, INCA MAX-50) and a high-resolution transmission electron microscope (HRTEM, JEM-2100F, JEOL) with energy dispersive X-ray spectroscopy (EDS, Oxford Link-Isis). The phase of sensing materials was checked with X-ray diffraction (XRD, D8-Advance, Bruker). The surface elemental composition was checked with X-ray photoelectron spectroscopy (XPS, Thermo ESCALAB 250XI). The sensor properties were measured by a gas-sensing test system (WS-60A, Weisheng Electronics, China). The devices were put into an airproof test box. Target gases such as TEA with calculated concentration were injected into the testing chamber by a microsyringe. The sensor response is defined as the ratio of R_a/R_g, where R_a and R_g are the resistances of the sensors in air and in target gas, respectively.

DOI: 10.1021/acsami.5b04904
ACS Appl. Mater. Interfaces 2015, 7, 19163−19171

3. RESULTS AND DISCUSSION

3.1. Characterizations of ZnO-Based Nanorods. Figure 1a schematically illustrates the fabrication process of the Au-SnO_2/ZnO nanorod sensor, which has been described in detail under Experimental Section. Panels b and c of Figure 1 exhibit the low-magnification SEM image of Al_2O_3 substrate with ZnO nanorods and the optical photograph of Au-SnO_2/ZnO gas sensor. The ZnO seed layer is important for the growth of ZnO nanorods. After the hydrothermal process, ZnO nanorods were directly grown on Al_2O_3 flat substrates, interdigitated with a pair of Au electrodes, Pt lead wires, and a heater. Moreover, the area coated with the ZnO seed layer shows a very high-density growth of nanorods. The SEM image of ZnO nanorods is shown in Figure 2a. ZnO nanorods grow nearly perpendicular to the substrate, and their diameters are about 50−100 nm with a hexagonal morphology. Figure 2b is the EDS spectrum of ZnO nanorods, and the peak of O and Zn can be clearly observed in this spectrum. No peaks are observed for other impurities, indicating the growth of pure ZnO nanorods. The peak of Al also can be observed in the spectrum, which is attributed to the Al_2O_3 substrate. Panels c and d of Figure 2 are SEM and EDS images of SnO_2/ZnO nanorods. The peak of Sn can also be seen clearly in the EDS apectrum. Figure 2e exhibits the SEM image of Au-SnO_2/ZnO nanorods. It shows that the ZnO nanorod morphology is preserved when it is covered with a thin layer of SnO_2 and Au nanoparticles on the surface. Figure 2f shows a high-magnification SEM image of Au-SnO_2/ZnO nanorods. The nanoparticles of Au also can be observed, which is consistent with its EDS spectrum shown in Figure 2g. The peaks of Au and Sn can be clearly observed. Figure 2h shows the XRD spectrum of as-synthesized ZnO, SnO_2/ZnO, and Au-SnO_2/ZnO nanorods. Typical wurtzite ZnO (JCPDS card 36-1451) diffraction patterns can be observed together with the diffraction peaks of Al_2O_3 substrate. When Au and SnO_2 were deposited onto ZnO nanorods, the XRD peaks of Au and SnO_2 could not be observed due to their small amount.

To gain further insights into the crystallographic features of pristine ZnO and Au-SnO_2/ZnO nanorods, TEM and associated electron diffraction techniques were employed. Figure 3a shows a low-magnification TEM image of a ZnO nanorod. The corresponding selected-area electron diffraction (SAED) pattern in the inset of Figure 3a confirms its highly

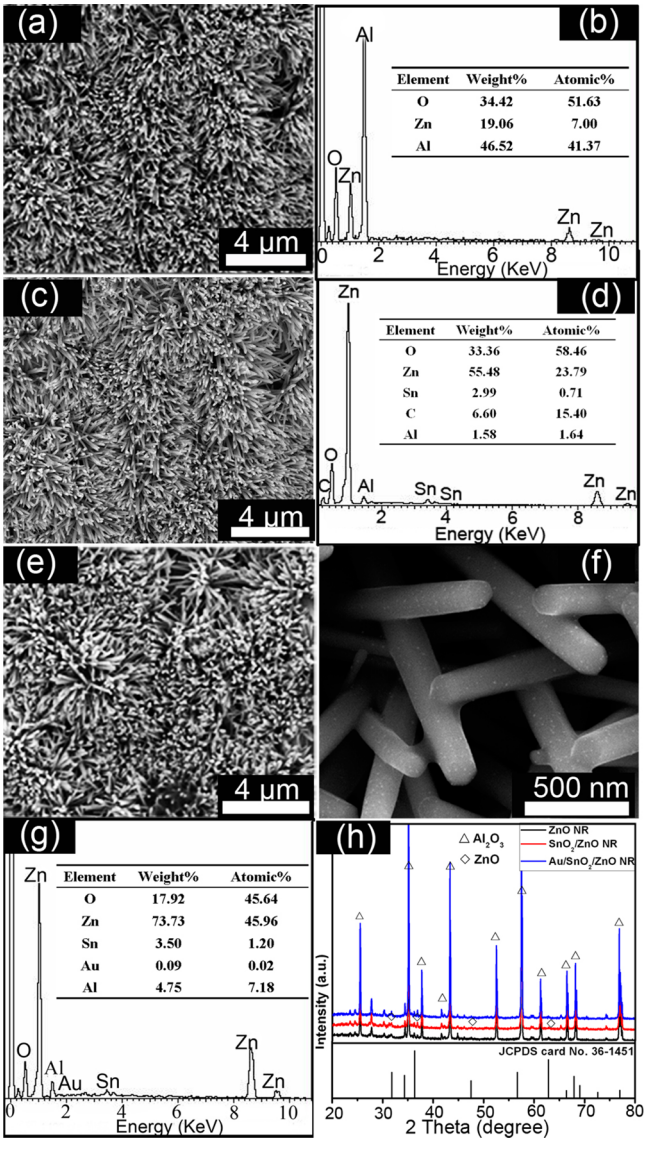

Figure 2. (a, b) SEM image of ZnO nanorods directly grown on Al_2O_3 substrate and corresponding EDS spectrum. (c, d) SEM image of SnO_2/ZnO nanorods and corresponding EDS spectrum. (e, f) SEM image of Au-SnO_2/ZnO nanorod after the implantation of SnO_2 shell and Au nanoparticles. (g) EDS spectrum of Au-SnO_2/ZnO nanorods. (h) XRD spectra of as-synthesized ZnO, SnO_2/ZnO, and Au-SnO_2/ZnO nanorods grown on Al_2O_3 substrate.

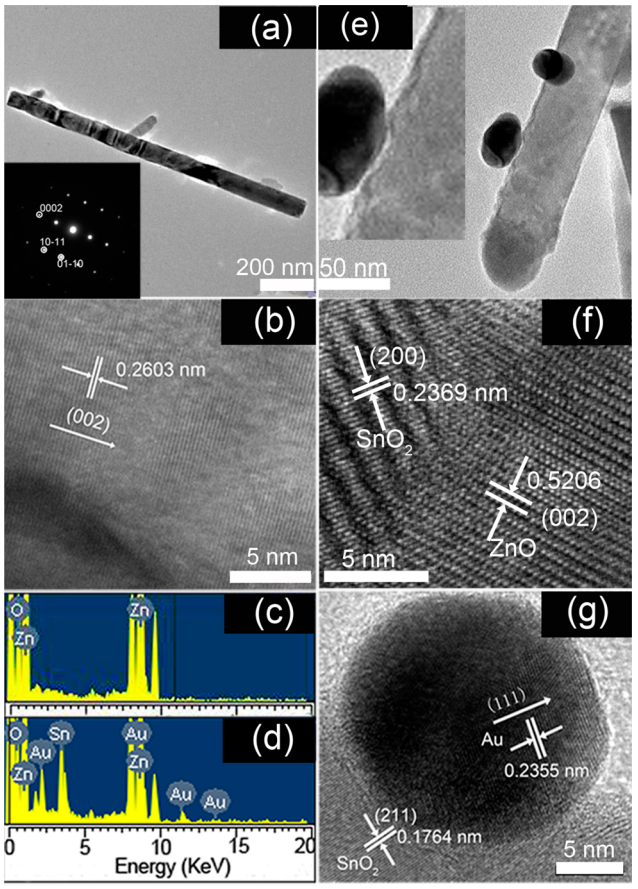

Figure 3. (a−c) TEM, HRTEM, and EDS images of ZnO nanorods. (d) EDS image of Au-SnO_2/ZnO nanorods. (e−g) TEM and HRTEM images of Au-SnO_2/ZnO nanorods.

DOI: 10.1021/acsami.5b04904
ACS Appl. Mater. Interfaces 2015, 7, 19163−19171

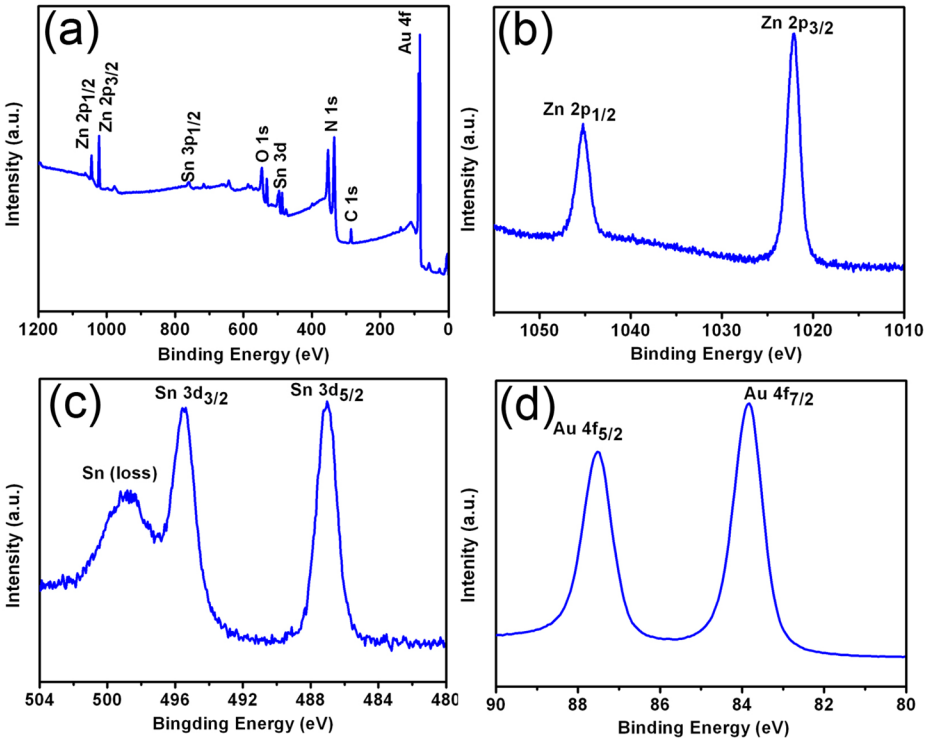

Figure 4. XPS spectra of the as-synthesized Au-SnO_2/ZnO nanorods: (a) XPS full survey spectrum; (b) Zn 2p spectrum; (c) Sn 3d spectrum; (d) Au 4f spectrum.

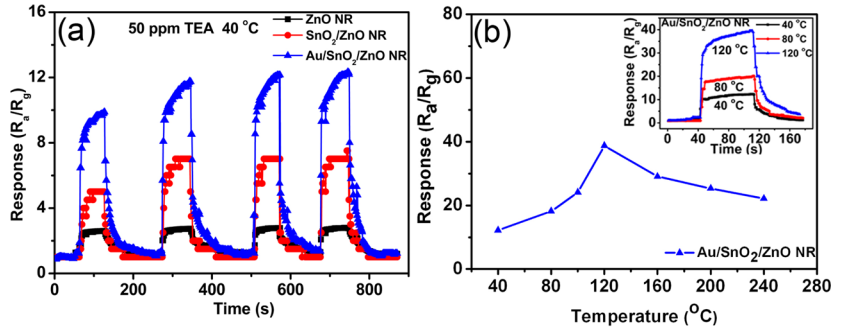

Figure 5. (a) Repeatability test of the sensors to 50 ppm of TEA at 40 °C. (b) Relationship between working temperature and response of Au-SnO_2/ZnO sensor to 50 ppm of TEA gas. (Inset) Response and recovery curves of Au-SnO_2/ZnO nanorod sensor at different working temperatures.

single-crystalline nature. The HRTEM analysis of a single ZnO nanorod (Figure 3b) reveals a well-resolved lattice with an interspacing of 0.2603 nm, which corresponds to the (0002) plane of the ZnO wurtzite structure.[30] Therefore, the nanorod growth axis is along the *c*-axis direction. Figure 3c is the EDS spectrum of the single ZnO nanorod, and similar composition information can be obtained as from Figure 2b of bulk nanorods.

Similar TEM, HRTEM, and electron diffraction analyses were also conducted on Au-SnO_2/ZnO nanorods. The EDS spectrum of a single Au-SnO_2/ZnO nanorod shown in Figure 3d reveals the presence of Au and SnO_2 on the ZnO nanorods. Figure 3e shows the TEM image of a Au-SnO_2/ZnO nanorod with a core−shell configuration of ZnO and SnO_2 and many small Au nanoparticles on its surface. Figure 3f shows the corresponding HRTEM image, where the lattice spacings are determined to be 0.2369 nm of SnO_2 (200) and 0.2603 nm of ZnO (002), respectively. The same HRTEM image evidently demonstrates that Au nanoparticles are present on the surface of SnO_2, as shown in Figure 3g. The *d*-spacing between adjacent lattice fringes in the Au nanoparticles is 0.2355 nm, which matches well with the Au (111) planes. The *d*-spacing (0.1764 nm) between the adjacent lattice fringes further confirms the appearance of intermediate SnO_2 shell layer.

The surface composition and structure of the as-synthesized Au-SnO_2/ZnO nanorod were further investigated with XPS as shown in Figure 4. In the XPS full survey spectrum of Figure 4a, the peaks of Zn, Sn, Au, O, and C elements can be observed clearly. The presence of C and N might be from hydrocarbons and nitrogen compounds in the synthesis. Panels b and c of Figure 4 display the high-resolution spectra for Zn and Sn species, respectively. The peaks of Figure 4b are centered at 1021.3 and 1044.8 eV, which are attributed to the Zn $2p_{3/2}$ and Zn $2p_{1/2}$ of Zn(II). The peaks appearing in Figure 4c are located at 486.4 and 495.2 eV and are ascribed to the Sn $3d_{5/2}$ and Sn $3d_{3/2}$ of Sn (IV), respectively.[31] Moreover, a peak of Sn (loss) appears on the high binding energy side of Sn $3d_{3/2}$. Figure 4d shows the high-resolution Au 4f spectrum of Au-

DOI: 10.1021/acsami.5b04904
ACS Appl. Mater. Interfaces 2015, 7, 19163−19171

SnO_2/ZnO samples. It shows a double feature with peaks centered at 83.9 and 87.7 eV, which correspond to the $4f_{7/2}$ and $4f_{5/2}$ signals of metallic Au (Au^0), respectively. The Au 4f peaks are relatively narrow and symmetrical, which indicates that there exists only one chemical state of Au in Au-SnO_2/ZnO nanorods.[32] Therefore, by combining SEM, EDS, TEM, and HRTEM data with XPS analysis, it can be confirmed again that a Au-loaded SnO_2 shell coated the surface of the ZnO nanorod.

3.2. Sensing Performance of ZnO-Based Nanorod Sensors. For sensing performances of ZnO-based nanorod sensors, the repeatability was first evaluated. Figure 5a shows typical response profiles of three kinds of gas sensors to 50 ppm of TEA at 40 °C. All sensors exhibit a reproducible run after four cycles, which demonstrates good device repeatability. Figure 5b shows the typical response of a Au-SnO_2/ZnO sensor to 50 ppm of TEA at operating temperatures from 40 to 240 °C. The maximum response to 50 ppm of TEA is about 40 at a higher temperature, for example, 120 °C, and then decreases with increasing operating temperature. Here, the best-performance working temperature is already much lower than typically reported data (~300 °C) for oxide semiconductor sensors.[27−29] However, the response is still up to 12.4 even at near room temperature (40 °C) with a heating voltage of 1.2 V. These can also be observed clearly in the inset of Figure 5b. As a low-powered gas sensor working at room temperature is always highly expected, the following response curves were all measured at 40 °C to further evaluate their sensing performance.

The response characteristics of three kinds of ZnO-based nanorod sensors toward different concentrations of TEA at 40 °C are shown in Figure 6a, and more control experimental data for SnO_2, Au-ZnO, and Au-SnO_2 sensors are presented in the Supporting Information (Figure S1). All of the sensor responses increased with increasing TEA concentration from 2 to 100 ppm. The Au-SnO_2/ZnO nanorod sensor increases more rapidly and exhibits the highest response values compared with other sensors. This can also be observed more clearly with Figure 6b. For the Au-SnO_2/ZnO nanorod with optimized SnO_2 shell thickness and Au nanoparticles, the sensor measured at 40 °C gets a response of 3.1 and 15.7 toward 2 and 100 ppm of TEA gas, respectively, which is about 4.8 times higher than that of the ZnO nanorod sensor (3.25 for 100 ppm). Moreover, the gas responses of the ZnO and ZnO/SnO_2 sensors tend to saturate quickly. This indicates the latter sensor performance exhibits better linear characteristic.

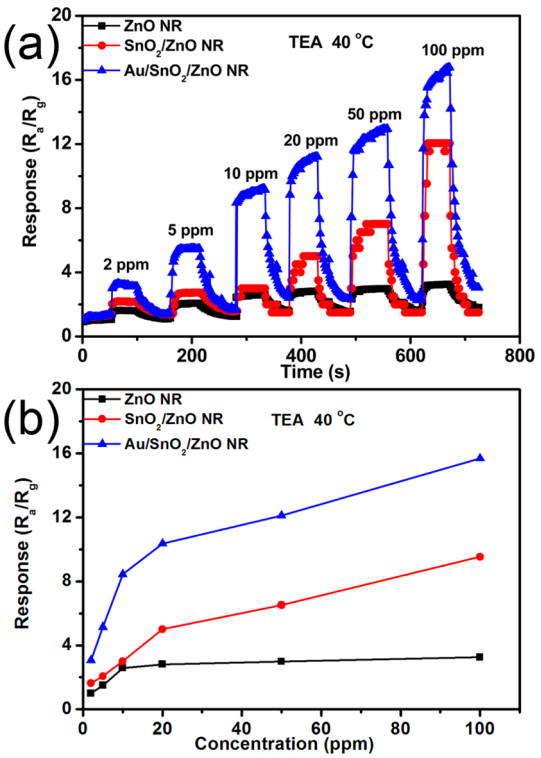

Figure 6. (a) Response and recovery curves of three kinds of sensors to TEA gas of different concentrations at 40 °C. (b) Corresponding relationship between sensor response and TEA concentration.

The response−recovery time, an important criterion for evaluating the performance of gas sensors, is also investigated. It is defined as the time taken by the sensor to achieve 90% of the total resistance change in the case of gas adsorption and desorption, respectively. Panels a−c of Figure 7 display the response and recovery curves of three typical sensors to 50 ppm of TEA at 40 °C. All sensors exhibit ultrafast response when TEA gas is injected into the box. As shown in Figure 7d, the response time of the Au-SnO_2/ZnO sensor is about 1.2 s. After desorption, all sensors need a longer time to recover to a steady state, which may be due to the low working temperature. As we already know, a chemical sensor working at a low temperature such as 40 °C is hardly reversible because the thermal energy is usually lower than the activation energy for gas desorption. This leads to a long recovery time.[33] However, by heating, it could recover quickly, as shown in the Supporting Information (Figure S2). In addition, with the deposition of Au nanoparticles and SnO_2 shells, the sensor resistances (time = 0) in air (R_a) increase gradually. This will be discussed in detail under Mechanism on the Enhanced Sensing Properties of Au-SnO2/ZnO Nanorods.

A comparison between the sensing performances of Au-SnO_2/ZnO nanorod sensors and some previously reported TEA gas sensors is summarized in Table 1 in terms of working temperature, response, and response−recovery time. A series of control experimental data on pristine ZnO, SnO_2, Au-ZnO, Au-SnO_2, and SnO_2/ZnO sensors are also presented. As can be seen, the Au-SnO_2/ZnO nanorod sensor exhibits near room working temperature, ultrafast response time, and relatively high response.

Selectivity is another important criterion of gas sensors. The responses of ZnO-, SnO_2/ZnO-, and Au-SnO_2/ZnO-based nanorod sensors to various volatile organic compounds, such as TEA, ethanol, acetone, 2-propanol, benzene, and *p*-xylene, are summarized in Figure 8. All gases were tested at a low operating temperature of 40 °C. As expected, the Au-SnO_2/ZnO nanorod sensor exhibits enhanced responses for each gas in comparison with that of the other two sensors. Moreover, the Au-SnO_2/ZnO sensor exhibited a bigger response for TEA, which is about 3.4 times higher than that of the pristine ZnO sensor, and its response to TEA is also higher than those interfering gases, indicating an impressive selectivity to TEA even at low working temperature. To further understand the influence of Au nanoparticles on selectivity, we also measured the selectivity of Au-SnO_2 toward different gases, as shown in the Supporting Information (Figure S3). It is found that only the catalytic effect of Au nanoparticles is not sufficient to design highly selective TEA sensor. Although the physical reason is still not very clear for us, enhanced selectivity for TEA was observed for Au-loaded ZnO/SnO_2 nanorods. One possible reason may be

DOI: 10.1021/acsami.5b04904
ACS Appl. Mater. Interfaces 2015, 7, 19163−19171

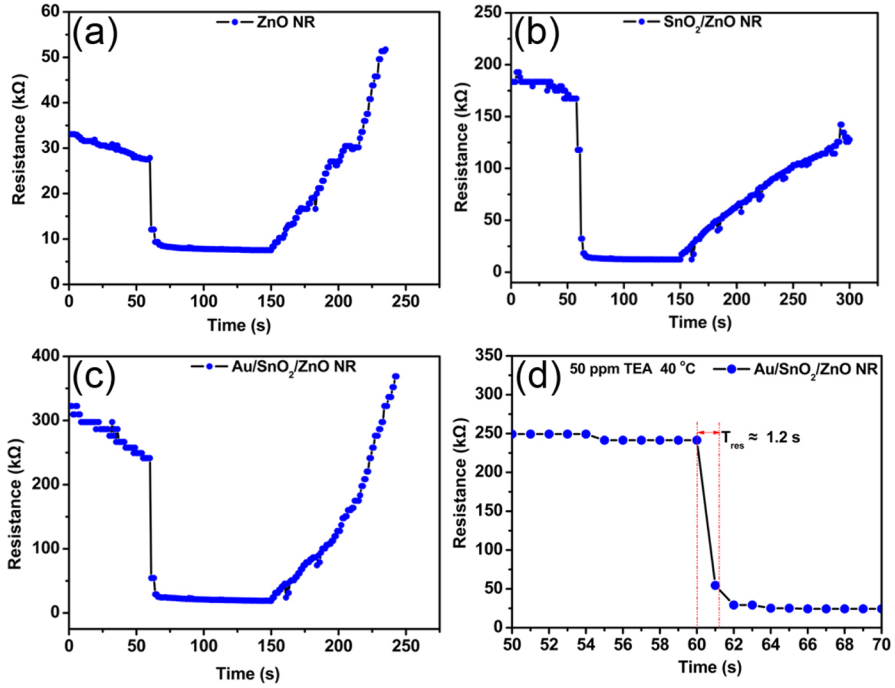

Figure 7. Response and recovery time of three sensors: (a) ZnO nanorod sensor; (b) SnO_2/ZnO nanorod sensor; (c) Au-SnO_2/ZnO nanorod gas sensor; (d) response time of Au-SnO_2/ZnO gas sensor taken from (c). The device resistivity at the beginning of measurement (time = 0 s) is the original sensor resistivity in air.

Table 1. TEA Sensing Properties of Our Work and Other Reported Oxide Semiconductor Gas Sensors Working under Different Operating Temperatures

material	gas concentration (ppm)	operating temperature (°C)	response (R_a/R_g)	$T_{response}$ (s)	$T_{recovery}$ (s)
SnO_2 nanorods[25]	1000 (TEA)	350	200	10	10
ZnO nanorods[34]	500 (TEA)	150	300	15	15
SnO_2 flowerlike[35]	100 (TEA)	350	4	<6	<6
$NiFe_2O_4$ nanorods[36]	100 (TEA)	175	100	22	
NiO/ZnO nanosheets[2]	100 (TEA)	320	300	7	33
SnO_2-ZnO nanocomposite[7]	100 (TMA)	330	200	10	30
ZnO film[37]	400 (TMA)	300	3.5		
ZnO nanorods	50 (TEA)	40	3	~1.1	~85
Au-ZnO nanorods	50 (TEA)	40	4	~1.3	~85
Au-SnO_2 nanosheets	50 (TEA)	40	7.1	~1.2	~70
SnO_2/ZnO nanorods	50 (TEA)	40	6.8	~2.0	~100
Au-SnO_2/ZnO nanorods	50 (TEA)	40	12.4	~1.2	~75

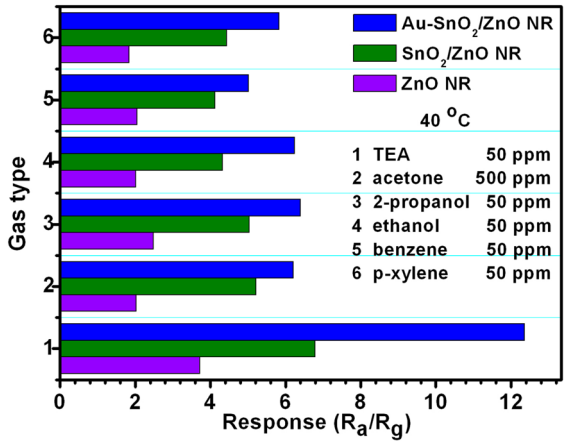

Figure 8. Selectivity comparison of three sensors for different target gases at 40 °C.

the different reaction activity of target gases in terms of bond energy.[2,38] The main bond energies of target gases, for example, TEA (C—N), 2-propanol (C—C), ethanol (O—H), benzene (C=C), and acetone (C=O), are 307, 345, 458.8, 610.3, and 798.9, kJ/mol, respectively.[2,38] Due to the low C—N bond energy, the high reaction activity of TEA molecules is expected to contribute to the high response of Au-SnO_2/ZnO sensors.

For real sensor applications, humidity is a prerequisite factor to be considered and shows important influence on the sensor performance.[39,40] Therefore, we also measured the gas-sensing characteristics at 40 °C under the wide relative humidity (RH) range from 19 to 66% to examine whether the sensing characteristics can be maintained in a highly humid condition. Figure 9a shows the relationship of sensor responses and RH. All of the sensor responses decrease with increasing RH. Moreover, when the RH is <40%, the sensor response decreases only slightly. Then, the response decreases quickly with further increase in RH. Such a response dependence on

DOI: 10.1021/acsami.5b04904
ACS Appl. Mater. Interfaces 2015, 7, 19163−19171

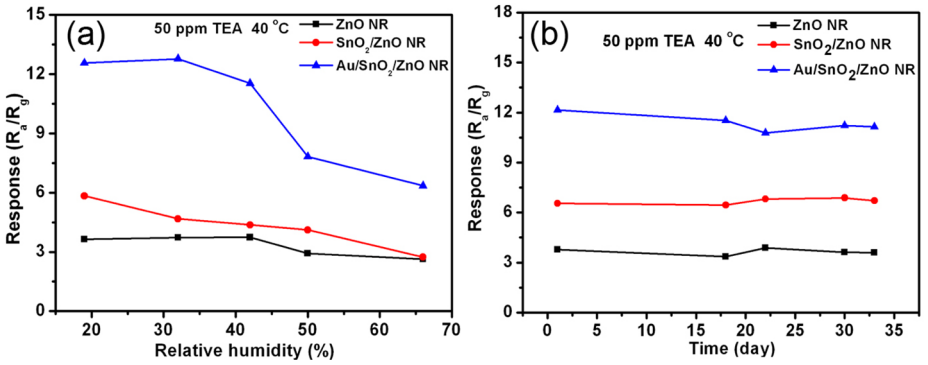

Figure 9. (a) Relationship between sensing response and relative humidity. (b) Long-term stability of the three sensors to 50 ppm of TEA at 40 °C.

RH is a general characteristic for metal oxide sensors. Several reasons have been proposed. First, the adsorption of water molecules leads to less chemisorption of oxygen species on the sensing material surface, which is responsible for the sensor response decrease.[37] Moreover, water molecules also act as a barrier against TEA adsorption. The superficial migration of the TEA on the Au-SnO_2/ZnO nanorod surface becomes difficult; thus, the response decreases.[41] Second, the reaction between the surface oxygen and the water molecules is conducive to a decrease in the sensor baseline resistance and results in a decrease of the response.[42] In addition, OH groups from water may be weak acceptors, competing with oxygen for the same adsorption sites and more easily accessible to the reaction with TEA.[43] The stability of three sensors over 1 month is also checked as shown in Figure 9b. Clearly, the sensors show nearly constant response to 50 ppm of TEA, which indicates high stability of the gas sensors.

3.3. Mechanism of the Enhanced Sensing Properties of Au-SnO_2/ZnO Nanorods. The basic sensing mechanism of n-type semiconductor sensors has been well documented with the space-charge or depletion layer model.[13,27,44,45] The adsorption and desorption of target gas molecules on the surface of sensing materials can effectively cause the resistance change of sensor devices. This is the basic working principle of oxide semiconductor sensors such as pure ZnO film or nanorod sensors. When the semiconductor heterojunctions such as P−N, N−N, or metal/semiconductor contact are formed on the surface of sensing materials, the enhanced sensor properties are already reported,[2,26−28,46,47] but the sensor working mechanism becomes rather complex and remains unclear.

As we know, the work functions of ZnO, SnO_2, and Au have been reported to be 5.2, 4.9, and 5.1 eV, respectively (Figure 10a).[45−48] Therefore, when the SnO_2 shell is coated onto the surface of a ZnO nanorod by PLD process, the N−N heterojunction will be formed between SnO_2 and ZnO. Thus, the electrons will flow from SnO_2 to ZnO until their Fermi levels equalize. This creates an electron depletion layer on the surface of SnO_2 and further bends the energy band and leads to a higher resistance state of sensing materials than of the pure ZnO nanorod sensor, which is proved by the sensor resistance in air as shown in Figure 7a,b. Moreover, when Au nanoparticles are loaded on the surface of SnO_2/ZnO core−shell nanorods, electrons flow further from SnO_2 to Au nanoparticles, which leads to the formation of Au-SnO_2 Schottky contact and widens the depletion layer on the SnO_2 shell. This further increases the device resistance of the SnO_2/ZnO nanorod sensor (Figure 7c). The energy band diagram of Au-SnO_2/ZnO heterojunctions is shown in Figure 10b.

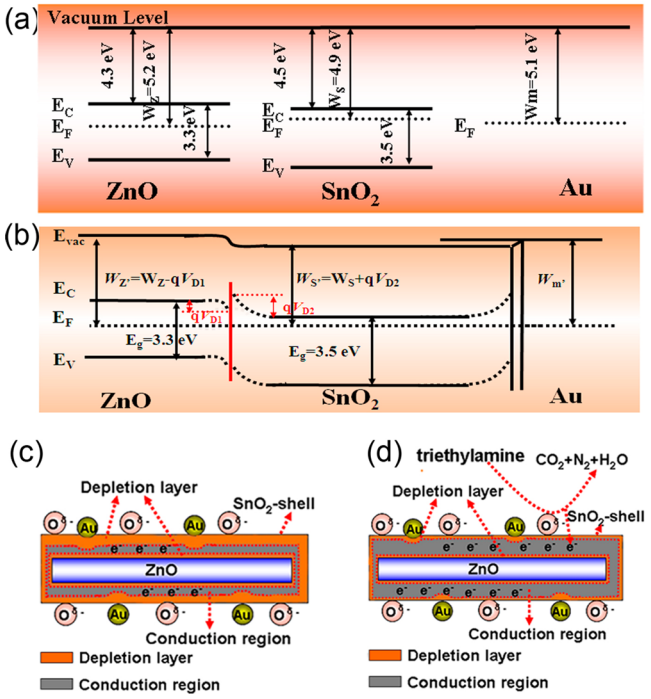

Figure 10. (a) Schematic diagram of the energy band configurations for ZnO, SnO_2, and Au. (b) Energy band diagram of Au-SnO_2/ZnO heterojunction. (c, d) Schematic model for the Au-SnO_2/ZnO sensor exposed to air and TEA gas, respectively. The outside part indicated by red dashed lines is the depletion layer.

Therefore, when Au-SnO_2/ZnO nanostructures are formed, the electrons in SnO_2 are greatly depleted due to the formation of Schottky contact and N−N heterojunction in addition to the adsorption of oxygen molecules. This causes a high resistance state of sensing materials, as shown in Figure 10c.

However, once Au-SnO_2/ZnO sensors are exposed to the reducing TEA gas, the interaction of TEA molecules with pre-adsorbed oxygen ions releases electrons back to Au-SnO_2/ZnO nanorods. The reaction between TEA and surface oxygen species can be simply described as[4,49]

$$(C_2H_5)_3N + O^{\delta-} \leftrightarrow CO_2 + H_2O + NO_2 + e^-$$

This significantly reduces the height of the Au-SnO_2 Schottky barrier and the width of the depletion layer between ZnO and SnO_2, resulting in a great decrease in sensor resistance, shown in Figure 10d. Thus, on the basis of the definition of sensor response ($S = R_a/R_g$), the enhanced response to TEA is mainly

DOI: 10.1021/acsami.5b04904
ACS Appl. Mater. Interfaces 2015, 7, 19163−19171

attributed to the variation of resistance caused by the formation of the SnO_2/ZnO junction and Au-SnO_2 Schottky barrier.

In addition, precious metal particle sensitized functions may be another reason for the enhancement of Au-SnO_2/ZnO nanorod's gas-sensing property. It has been reported that the use of precious metals, as an active component, can improve sensor performance, mainly due to the catalytic effect of precious metals.[47,50] Au nanoparticles may catalyze and accelerate the dissociation of oxygen molecules on the surface of SnO_2, which also enhances the Au-SnO_2/ZnO sensor performance.

4. CONCLUSIONS

In summary, we report a near room temperature and fast-response TEA gas sensor by designing Au-SnO_2/ZnO nanorods, and their sensing mechanism is also discussed in detail. With the introduction of a seed layer, ZnO nanorods grew directly on Al_2O_3 flat electrodes with a simple and cost-effective hydrothermal process. By employing PLD and sputtering method, the construction of Au-SnO_2/ZnO nanorod heterostructure is highly controllable and reproducible. Such a gas sensor can work at temperatures as low as 40 °C and exhibit fast response (~1.2 s) and high response (12.4) to 50 ppm of TEA gas, which are much higher than those of pristine ZnO nanorod sensors. In air, the formation of a depletion layer due to Au/SnO_2 Schottky contact and SnO_2/ZnO N−N heterojunction greatly increases the sensor resistance in comparison with a pristine ZnO sensor. This is the main reason for the enhanced response to TEA. This study provides a rational way for the design and fabrication of chemiresistance gas sensors with high performance.

■ ASSOCIATED CONTENT

Supporting Information

The Supporting Information is available free of charge on the ACS Publications website at DOI: 10.1021/acsami.5b04904.

Response comparison of ZnO, Au-ZnO, and Au-SnO_2 sensors, response−recovery curves of the Au-SnO_2/ZnO nanorod working at different temperatures; selectivity of the Au-SnO_2 sensor (PDF)

■ AUTHOR INFORMATION

Corresponding Author

*(B.-Q.C.) E-mail: mse_caobq@ujn.edu.cn. Fax: +86-531-8797-4453. Phone: +86-531-8973-6292.

Notes

The authors declare no competing financial interest.

■ ACKNOWLEDGMENTS

This work is supported by NSFC (11174112) and Shandong Provincial Science Foundation (JQ201214, 2014ZRB019JP, ZR2015BQ006). Research programs from the Ministry of Education, China, are also acknowledged (NCET-11-1027, 213021A). B.-Q.C. thanks the Taishan Scholar Chaired Professorship tenured at University of Jinan.

■ REFERENCES

(1) Liu, B.; Zhang, L. H.; Zhao, H.; Chen, Y.; Yang, H. Q. Synthesis and Sensing Properties of Spherical Flowerlike Architectures Assembled with SnO_2 Submicron Rods. *Sens. Actuators, B* **2012**, *173*, 643−651.

(2) Ju, D.; Xu, H.; Qiu, Z.; Guo, J.; Zhang, J.; Cao, B. Highly Sensitive and Selective Triethylamine-Sensing Properties of Nanosheets Directly Grown on Ceramic Tube by Forming NiO/ZnO PN Heterojunction. *Sens. Actuators, B* **2014**, *200*, 288−296.

(3) Chen, E. X.; Fu, H. R.; Lin, R.; Tan, Y. X.; Zhang, J. Highly Selective and Sensitive Trimethylamine Gas Sensor Based on Cobalt Imidazolate Framework Material. *ACS Appl. Mater. Interfaces* **2014**, *6*, 22871−22875.

(4) Wang, J.; Yu, L.; Wang, H.; Ruan, S.; Li, J.; Wu, F. Preparation and Triethylamine Sensing Properties of Ce Doped In_2O_3 Nanofibers. *Acta. Phys.−Chim. Sin.* **2010**, *26*, 3101−3105.

(5) Gandu, B.; Sandhya, K.; Rao, A. G.; Swamy, Y. V. Gas Phase Bio-Filter for the Removal of Triethylamine (TEA) from Air: Microbial Diversity Analysis with Reference to Design Parameters. *Bioresour. Technol.* **2013**, *139*, 155−160.

(6) Haskin, J. F.; Warren, G. W.; Priestley, L. J. Gas Chromatography Determination of Constituents in the Study of Azeotropes. *Anal. Chem.* **1958**, *30*, 217−219.

(7) Zhang, W. H.; Zhang, W. D. Fabrication of SnO_2−ZnO Nanocomposite Sensor for Selective Sensing of Trimethylamineand the Freshness of Fishes. *Sens. Actuators, B* **2008**, *134*, 403−408.

(8) Nohta, H.; Satozono, H.; Koiso, K.; Yoshida, H.; Ishida, J.; Yamaguchi, M. Highly Selective Fluorometric Determination of Polyamines Based on Intramolecular Excimer-Forming Derivatization with a Pyrene-Labeling Reagent. *Anal. Chem.* **2000**, *72*, 4199−4204.

(9) Filippo, E.; Mannob, D.; Buccolieri, A.; Serra, A. Green Synthesis of Sucralose-Capped Silver Nanoparticles for Fast Colorimetric Triethylamine Detection. *Sens. Actuators, B* **2013**, *178*, 1−9.

(10) Law, M.; Kind, H.; Messer, B.; Kim, F.; Yang, P. Photochemical Sensing of NO_2 with SnO_2 Nanoribbon Nanosensors at Room Temperature. *Angew. Chem., Int. Ed.* **2002**, *41*, 2405−2408.

(11) Dai, Z. F.; Xu, L.; Duan, G. T.; Li, T.; Zhang, H. W.; Li, Y.; Wang, Y.; Wang, Y. L.; Cai, W. P. Fast-Response, Sensitivitive and Low-Powered Chemosensors by Fusing Nanostructured Porous Thin Film and IDEs-Microheater Chip. *Sci. Rep.* **2013**, *3*, 1669.

(12) Kuang, Q.; Lao, C. S.; Wang, Z. L.; Xie, Z. X.; Zheng, L. S. High-Sensitivity Humidity Sensor Based on a Single SnO_2 Nanowire. *J. Am. Chem. Soc.* **2007**, *129*, 6070−6071.

(13) Ju, D.; Xu, H.; Zhang, J.; Guo, J.; Cao, B. Direct Hydrothermal Growth of ZnO Nanosheets on Electrode for Ethanol Sensing. *Sens. Actuators, B* **2014**, *201*, 444−451.

(14) Gyger, F.; Hübner, M.; Feldmann, C.; Barsan, N.; Weimar, U. Nanoscale SnO_2 Hollow Spheres and Their Application as a Gas-Sensing Material. *Chem. Mater.* **2010**, *22*, 4821−4827.

(15) Wang, J. J.; Wang, Z. Y.; Liu, C. J. Enhanced Activity for CO Oxidation Over WO_3 Nanolamella Supported Pt Catalyst. *ACS Appl. Mater. Interfaces* **2014**, *6*, 12860−12867.

(16) Kim, H. J.; Jeong, H. M.; Kim, T. H.; Chung, J. H.; Kang, Y. C.; Lee, J. H. Enhanced Ethanol Sensing Characteristics of In_2O_3-Decorated NiO Hollow Nanostructures Via Modulation of Hole Accumulation Layers. *ACS Appl. Mater. Interfaces* **2014**, *6*, 18197−18204.

(17) Xiao, Y. H.; Lu, L. Z.; Zhang, A. Q.; Zhang, Y. H.; Sun, L.; Huo, L.; Li, F. Highly Enhanced Acetone Sensing Performances of Porous and Single Crystalline ZnO Nanosheets: High Percentage of Exposed (100) Facets Working Together with Surface Modification with Pd Nanoparticles. *ACS Appl. Mater. Interfaces* **2012**, *4*, 3797−3804.

(18) Kim, J.; Yong, K. Mechanism Study of ZnO Nanorod Bundle Sensors for H_2S Gas Sensing. *J. Phys. Chem. C* **2011**, *115*, 7218−7224.

(19) Xu, Z. K.; Duan, G. T.; Li, Y.; Liu, G. Q.; Zhang, H. W.; Dai, Z. F.; Cai, W. P. CuO−ZnO Micro/Nanoporous Array-Film-Based Chemosensors: New Sensing Properties to H_2S. *Chem. - Eur. J.* **2014**, *20*, 6040−6046.

(20) Jing, Z. H.; Zhan, J. H. Fabrication and Gas-Sensing Properties of Porous ZnO Nanoplates. *Adv. Mater.* **2008**, *20*, 4547−4551.

(21) Youn, S. K.; Ramgir, N.; Wang, C.; Subannajui, K.; Cimalla, V.; Zacharias, M. Catalyst-Free Growth of ZnO Nanowires Based on Topographical Confinement and Preferential Chemisorption and

DOI: 10.1021/acsami.5b04904
ACS Appl. Mater. Interfaces 2015, 7, 19163−19171

Their Use for Room Temperature CO Detection. *J. Phys. Chem. C* **2010**, *114*, 10092−10100.
(22) An, W.; Wu, X. J.; Zeng, X. C. Adsorption of O_2, H_2, CO, NH_3, and NO_2 on ZnO Nanotube: A Density Functional Theory Study. *J. Phys. Chem. C* **2008**, *112*, 5747−5755.
(23) Talwar, V.; Singh, O.; Singh, R. C. ZnO Assisted Polyaniline Nanofibers and Its Application as Ammonia Gas Sensor. *Sens. Actuators, B* **2014**, *191*, 276−282.
(24) Kim, J.; Yong, K. Mechanism Study of ZnO Nanorod-Bundle Sensors for H_2S Gas Sensing. *J. Phys. Chem. C* **2011**, *115*, 7218−7224.
(25) Wang, D.; Chu, X. F.; Gong, M. L. Gas-Sensing Properties of Sensors Based on Single-Crystalline SnO_2 Nanorods Prepared by a Simple Molten-Salt Method. *Sens. Actuators, B* **2006**, *117*, 183−187.
(26) Park, S.; An, S.; Mun, Y.; Lee, C. UV-Enhanced NO_2 Gas Sensing Properties of SnO_2−Core/ZnO-Shell Nanowires at Room Temperature. *ACS Appl. Mater. Interfaces* **2013**, *5*, 4285−4292.
(27) Li, X.; Zhou, X.; Guo, H.; Wang, C.; Liu, J.; Sun, P.; Liu, F.; Lu, G. Design of Au@ZnO Yolk−Shell Nanospheres with Enhanced Gas Sensing Properties. *ACS Appl. Mater. Interfaces* **2014**, *6*, 18661−18667.
(28) Tang, W.; Wang, J.; Yao, P.; Li, X. Hollow Hierarchical SnO_2-ZnO Composite Nanofibers with Heterostructure Based on Electrospinning Method for Detecting Methanol. *Sens. Actuators, B* **2014**, *192*, 543−549.
(29) Kaneti, Y. V.; Zakaria, Q. M. D.; Zhang, Z.; Chen, C.; Yue, J.; Liu, M.; Jiang, X.; Yu, A. Solvothermal Synthesis of ZnO-Decorated a-Fe_2O_3 Nanorods with Highly Enhanced Gas-Sensing Performance Toward *n*-Butanol. *J. Mater. Chem. A* **2014**, *2*, 13283−13292.
(30) Qiu, Z. W.; Yang, X.; Han, J.; Zhang, P.; Cao, B.; Dai, Z.; Duan, G.; Cai, W. Sodium-Doped ZnO Nanowires Grown by High-Pressure PLD and Their Acceptor-Related Optical Properties. *J. Am. Ceram. Soc.* **2014**, *97*, 2177−2184.
(31) Zhang, Z.; Yang, Z.; Wang, R.; Feng, Z.; Xie, X.; Liao, Q. Electrochemical Performance of ZnO/SnO_2 Composites as Anode Materials for Zn/Ni Secondary Batteries. *Electrochim. Acta* **2014**, *134*, 287−292.
(32) Liu, C.; Kuang, Q.; Xie, Z.; Zheng, L. The Effect of Noble Metal (Au, Pd and Pt) Nanoparticles on the Gas Sensing Performance of SnO_2-Based Sensors: a Case Study on the {221} High-Index Faceted SnO_2 Octahedra. *CrystEngComm* **2015**, *17*, 6308.
(33) Fan, Z. Y.; Lu, J. G. Gate-Refreshable Nanowire Chemical Sensors. *Appl. Phys. Lett.* **2015**, *86*, 123510.
(34) Lv, Y. Z.; Li, C. R.; Guo, L.; Wang, F. C.; Xu, Y.; Chu, X. F. Triethylamine Gas Sensor Based on ZnO Nanorods Prepared by a Simple Solution Route. *Sens. Actuators, B* **2009**, *141*, 85−88.
(35) Chu, X. F.; Jiang, D. L.; Zheng, C. M. The Preparation and Gas-Sensing Properties of $NiFe_2O_4$ Nanocubesand Nanorods. *Sens. Actuators, B* **2007**, *123*, 793−797.
(36) Roy, S.; Basu, S. ZnO Thin Film Sensors for Detecting Dimethyl- and Trimethylamine Vapors. *J. Mater. Sci.: Mater. Electron.* **2004**, *15*, 321−326.
(37) Park, S. H.; Ryu, J. Y.; Choi, H. H.; Kwon, T. H. Zinc Oxide Thin Film Doped with Al_2O_3, TiO_2 and V_2O_5 as Sensitive Sensor for Trimethylamine Gas. *Sens. Actuators, B* **1998**, *46*, 75−79.
(38) Zhang, L. X.; Zhao, J. H.; Lu, H. Q.; Li, L.; Zheng, J. F.; Zhang, J.; Li, H.; Zhu, Z. P. Highly Sensitive and Selective Dimethylamine Sensors Based on Hierarchical ZnO Architectures Composed of Nanorods and Nanosheet Assembled Microspheres. *Sens. Actuators, B* **2012**, *171−172*, 1101−1109.
(39) Hong, H.-S.; Chung, G.-S. Controllable Growth of Oriented ZnO Nanorods Using Ga-Doped Seed Layers and Surface Acoustic Wave Humidity Sensor. *Sens. Actuators, B* **2014**, *195*, 446−451.
(40) Chen, E. X.; Yang, H. Y.; Zhang, J. Zeolitic Imidazolate Framework as Formaldehyde Gas Sensor. *Inorg. Chem.* **2014**, *53*, 5411−5413.
(41) Wang, C.; Yin, L.; Zhang, L.; Xiang, D.; Gao, R. Metal Oxide Gas Sensors: Sensitivity and Influencing Factors. *Sensors* **2010**, *10*, 2088−2106.
(42) Gong, J.; Chen, Q.; Lian, M.; Liu, N.; Stevenson, R. G.; Adamic, F. Micromachined Nanocrystalline Silver Doped SnO_2 H_2S Sensor. *Sens. Actuators, B* **2006**, *114*, 32−39.
(43) Barsan, N.; Weimar, U. Understanding the Fundamental Principles of Metal Oxide Based Gas Sensors; the Example of CO Sensing with SnO_2 Sensors in the Presence of Humidity. *J. Phys.: Condens. Matter* **2003**, *15*, 813−839.
(44) Li, Z. P.; Zhao, Q. Q.; Fan, W. L.; Zhan, J. H. Porous SnO_2 Nanospheres as Sensitive Gas Sensors for Volatile Organic Compounds Detection. *Nanoscale* **2011**, *3*, 1646−1652.
(45) Chiu, H. C.; Yeh, C. S. Hydrothermal Synthesis of SnO_2 Nanoparticles and Their Gas-Sensing of Alcohol. *J. Phys. Chem. C* **2007**, *111*, 7256−7259.
(46) Mondala, B.; Basumatari, B.; Dasb, J.; Roychaudhury, C.; Saha, H.; Mukherjee, N. ZnO−SnO_2 Based Composite Type Gas Sensor for Selective Hydrogen Sensing. *Sens. Actuators, B* **2014**, *B194*, 389−396.
(47) Ramgir, N. S.; Sharma, P. K.; Datta, N.; Kaur, M.; Debnath, A. K.; Aswal, D. K.; Gupta, S. K. Room Temperature H_2S Sensor Based on Au Modified ZnO Nanowires. *Sens. Actuators, B* **2013**, *186*, 718−726.
(48) Ju, D.; Xu, H.; Xu, Q.; Gong, H. B.; Qiu, Z.; Guo, J.; Zhang, J.; Cao, B. High Triethylamine-Sensing Properties of NiO/SnO_2 Hollow Sphere P-N Heterojunction Sensors. *Sens. Actuators, B* **2015**, *215*, 39−44.
(49) Takao, Y.; Nakanishi, M.; Kawaguchi, T.; Shimizu, Y.; Egashira, M. Semiconductor Dimethylamine Gas Sensors with High Sensitivity and Selectivity. *Sens. Actuators, B* **1995**, *24−25*, 375−379.
(50) Yamazoe, N. New Approaches for Improving Semiconductor Gas Sensors. *Sens. Actuators, B* **1991**, *5*, 7−19.

DOI: 10.1021/acsami.5b04904
ACS Appl. Mater. Interfaces 2015, 7, 19163−19171